




Chemical and mineral comparison of fossil insect cuticles from Crato *Konservat Lagerstätte*, Lower Cretaceous of Brazil

Francisco Irineudo Bezerra¹  · João H. da Silva² · Emílio de Castro Miguel³ · Alexandre R. Paschoal⁴ · Daniel R. Nascimento Jr.¹ · Paulo T. C. Freire⁴ · Bartolomeu C. Viana⁵ · Márcio Mendes¹

Received: 6 July 2019 / Accepted: 10 January 2020 / Published online: 24 January 2020
© Universidad Complutense de Madrid 2020

Abstract

The Crato Formation palaeoentomofauna from the Lower Cretaceous (Aptian) of northeast Brazil is extremely well preserved. Crato insects are often complete with abdomen, thorax, head, legs, wings articulated and fragile cuticle details observed at the macro and micro scale. The Crato Formation stands out for the high diversity of fossil insects with at least 386 described species, so far. We investigate the preservation pathways through SEM–EDS and Raman spectroscopy, which give fundamental insights regarding the understanding of this complex theme. Our study compared cuticle soft-tissue preservation of *Ensifera* in different layers of the Crato limestone. The results of our analyses confirmed that the anaerobic bacterial respiration processes influenced the labile-tissues preservation. *Ensifera* fossils display preservational stages ranging from kerogenization to pyritization. Kerogenization represents the partial or complete chemical transformation of organic material into aliphatic and cyclic hydrocarbons in situ during mesodiagenesis, while pyritization occurs during the decaying of carcass in the early diagenesis. Here, we followed the previous hypothesis of fish tissue preservation that these processes are governed principally by variations in the positioning and residence time of the carcasses in different microbial zones within the sediment column. Besides early/mesodiagenetic modifications, oxidation processes during recent weathering led to some mineral transformations that played a key role in the preservation of *Ensifera*.

Keywords Crato Formation · Kerogenization · Pyritization · *Ensifera*

Resumen

La paleoentomofauna de La Formación Crato, Cretáceo Inferior (Aptiano) del Nordeste de Brasil, está extremadamente bien preservada. En general, los insectos de Crato se completan con abdomen, tórax, cabeza, piernas, alas articuladas y detalles frágiles de la cutícula observados en escalas macro y micro. La Formación Crato se destaca por la alta diversidad de fósiles

Electronic supplementary material The online version of this article (<https://doi.org/10.1007/s41513-020-00119-y>) contains supplementary material, which is available to authorized users.

✉ Francisco Irineudo Bezerra
irineudoufc@gmail.com

- ¹ Departamento de Geologia, Universidade Federal do Ceará, Fortaleza, Ceará 64049-550, Brasil
- ² Campus de Juazeiro do Norte, Universidade Federal do Cariri, Juazeiro do Norte, Ceará 63000-000, Brasil
- ³ Departamento de Engenharia Metalúrgica e de Materiais, Universidade Federal do Ceará, Fortaleza, Ceará 60020-181, Brasil
- ⁴ Departamento de Física, Universidade Federal do Ceará, Fortaleza, Ceará 60455-970, Brasil
- ⁵ Departamento de Física, Universidade Federal do Piauí, Teresina, Piauí 64048-480, Brasil

de insectos con al menos 386 especies descritas, hasta ahora. En este trabajo se investigó las vías de preservación a través de MEV-EDX y Espectroscopia Raman, que proporcionan informaciones fundamentales sobre la comprensión de este tema complejo. Este estudio comparó la preservación de tejidos blandos de las cutículas de Ensifera, en diferentes capas de rocas carbonáticas de La Formación Crato. Los resultados confirman que los procesos anaeróbicos de respiración bacteriana influenciaron la preservación de los tejidos lábiles. Los fósiles de Ensifera exhiben modos de preservación que van desde la querogenización a la piritización. La querogenización representa la transformación química parcial o completa del material orgánico en hidrocarburos alifáticos y cíclicos in situ durante la mesodiagénesis, mientras que la piritización ocurre durante la descomposición de la carcasa en la eodiagénesis. Aquí, se sigue la hipótesis sobre la preservación del tejido de los peces de que estos procesos de son influenciados por variaciones en la ubicación y tiempo de residencia de las carcasas en diferentes zonas microbianas, dentro de la columna de sedimentos. Además de las modificaciones eodiagenéticas y mesogenéticas, los procesos de oxidación durante el intemperismo reciente llevaron a algunas transformaciones minerales que desempeñaron un papel fundamental en la preservación de los Ensifera.

Palabras clave Formación Crato · Querogenización · Piritización · Ensifera

1 Introduction

Fossil insects have been taxonomically studied to date, but details on their fossil diagenesis are still far from understood. However, remarkable progress has been made in insect taphonomy investigations (Zhehikhin 2002; Martínez-Delclòs et al. 2004; Smith et al. 2006; Smith and Moe-Hoffman 2007; McNamara et al. 2011; Thoene-Henning et al. 2012; McNamara et al. 2012; Wang et al. 2012; McNamara 2013; Pan et al. 2014; Barling et al. 2015; Greenwalt et al. 2015; Osés et al. 2016; Anderson and Smith 2017; Dias and Carvalho 2020). The preservation of organisms depends on the type of tissue, rate of decay, low energy, reduced-oxygen, rapid growth of authigenic minerals, time and depth of burial and geochemical conditions during and after that (Briggs 2003; Briggs and McMahon 2006; Cai et al. 2012; Forchielli et al. 2014). Thus, fossil deposits with exceptional preservation are extremely important to understand the taphonomic pathways that allow the preservation of delicate tissues.

The Araripe Basin stands out from others in the mainland Northeast Brazil because it encompasses the most complete Cretaceous geological record and, mainly, for its paleontological content. The Crato Formation, Lower Cretaceous, is known worldwide as a *Konservat-Lagerstätte* due to its well-preserved fossil record in a lacustrine paleoenvironment (Martill and Bechly 2007). The fossils are relatively abundant and diverse, including vertebrates, invertebrates, plants, trace fossils and palynomorphs (Viana and Neumann 2000). The Crato insects are commonly complete, often three-dimensionally, and thus reveal details like abdominal segmentation, thoracic appendages, wings displaying well defined venation and head appendages (e.g., antennae) (Barling et al. 2015). The rich paleontomofauna of this unit is a taphonomic window for the lower Cretaceous (Soares et al. 2013), justifying the study of its fossils. The Crato Fm. deposit is regarded as one of the largest in taxonomic diversity and number of individual Cretaceous insects (Grimaldi

1990), being represented with the orders of Orthoptera, Ensifera, Isoptera, Homoptera, Hymenoptera, Blattodea, Ephemeroptera, Odonata, Dermaptera, Raphidioptera, Diptera, Trichoptera, Coleoptera, Neuroptera and Heteroptera. Among them, Ensifera is highlighted in terms of number of individuals. From the four known superfamilies, two (Grylloidea and Hagloidea) have been noticed in the Crato Fm. (Heads and Martins-Neto 2007).

An intimate relationship is observed between insect soft-tissue preservation and fine-grained laminated carbonates (Martínez-Delclòs et al. 2004). Many other localities that are rich in finely laminated carbonates, such as Solnhofen (Germany), Las Hoyas and Montsec (Spain) and Green River (USA), also preserve a diverse fossil insect assemblage. The Crato's limestone is traditionally attributed to chemical precipitation associated with fine terrigenous sediments affected by a microbial organic mediation (Catto et al. 2016). According to Neumann et al. (2003), two laminated limestone facies (microfacies) occur in the Crato Limestone: clay-carbonate rhythmite ('dark') and laminated limestone ('pale', dominated by calcite crystals), that correspond to a shift in the depositional balance of authigenic carbonate precipitation and terrigenous input (Heimhofer and Martill 2007). The clay-carbonate rhythmite displays (compared with laminated limestone) higher organic matter/clay content, peloids and pyrite occurring in scattered layers, thus suggesting that they were deposited during higher terrigenous influence (Neumann et al. 2003). In contrast, the laminated limestone shows a higher calcium content and lower organic matter/clay accumulation, thus suggesting that they were deposited in the most distal part of the lacustrine setting (Heimhofer et al. 2010). In fact, a notable feature of the Crato carbonates is their color pattern, in most quarries the color pattern of limestones varies between blue to dark gray and light yellow to orange. The occurrence of reddish limestones in the Crato Formation can represent a late telodiagenetic stage (Heimhofer and Martill 2007; Menon and

Martill 2007). Microfractures filled by iron oxide minerals further supports the secondary alteration under influence of meteoric waters affecting the limestone (Cabral et al. 2019). There is no evidence for strong mechanical compaction in the Crato limestone, implying a shallow burial and low thermal alteration (Heimhofer and Martill 2007; Nascimento Jr et al. 2016; Santos et al. 2017).

In this work, we analyze *Ensifera* (crickets) fossils from different sedimentary layers of the Crato Formation. Besides the typical light yellow and dark gray limestone colors (Heimhofer and Martill 2007), we also included a variety of reddish limestone [(Fig. 1b—dark-gray limestone (DL); c—yellow limestone (YL); d—red limestone (RL)]. Our main goal is to investigate the preservation of fragile morphological structures at the cellular level as well as cuticular soft tissues preserved as mineral replacements subsequently affected by diagenetic alterations. We intend to integrate most these features to geobiological and post-diagenetic (weathering) processes, contributing with additional information on the previous taphonomic model (Osés

et al. 2017) about the exceptional preservation of fossils in the Crato Formation.

2 Geological setting

The Araripe Basin is located in the border area of the Brazilian states of Piauí, Ceará, Paraíba and Pernambuco, covering an area of approximately 9000 km².

The sedimentary evolution of this basin is related to the Gondwana rifting event and the opening of the South Atlantic Ocean (Matos 1999). The Araripe Basin is limited in the south by the Pernambuco Lineament and in the north by the Patos Lineament, both oriented in an almost E–W direction (Ponte and Ponte Filho 1996). Gravimetric, magneto-metric and seismic studies indicate reactivation of ancient NE–SW lineaments that was responsible for the development of a horst-graben system under the basin, originating the Feira Nova and Cariri sub-basins separated by the Dom Leme High (Ponte and Ponte Filho 1996). The stratigraphic

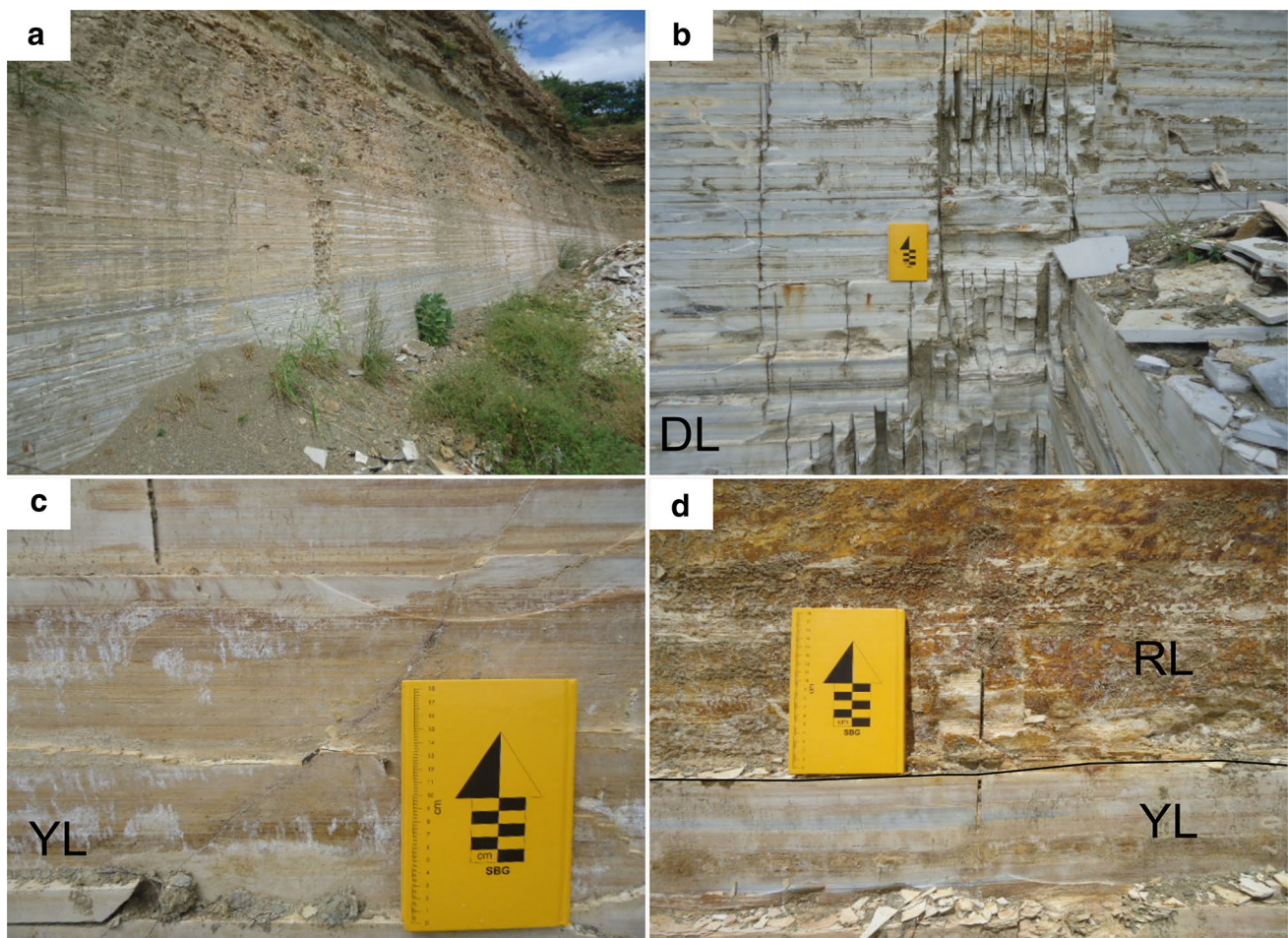


Fig. 1 Distinct coloration patterns observed in the Crato Formation limestones (a), general view of the quarry located in Nova Olinda, Ceará State (b), dark-gray limestone layers (DL) (c) yellow limestone layers (YL) (d), Reddish limestone layers (RL)

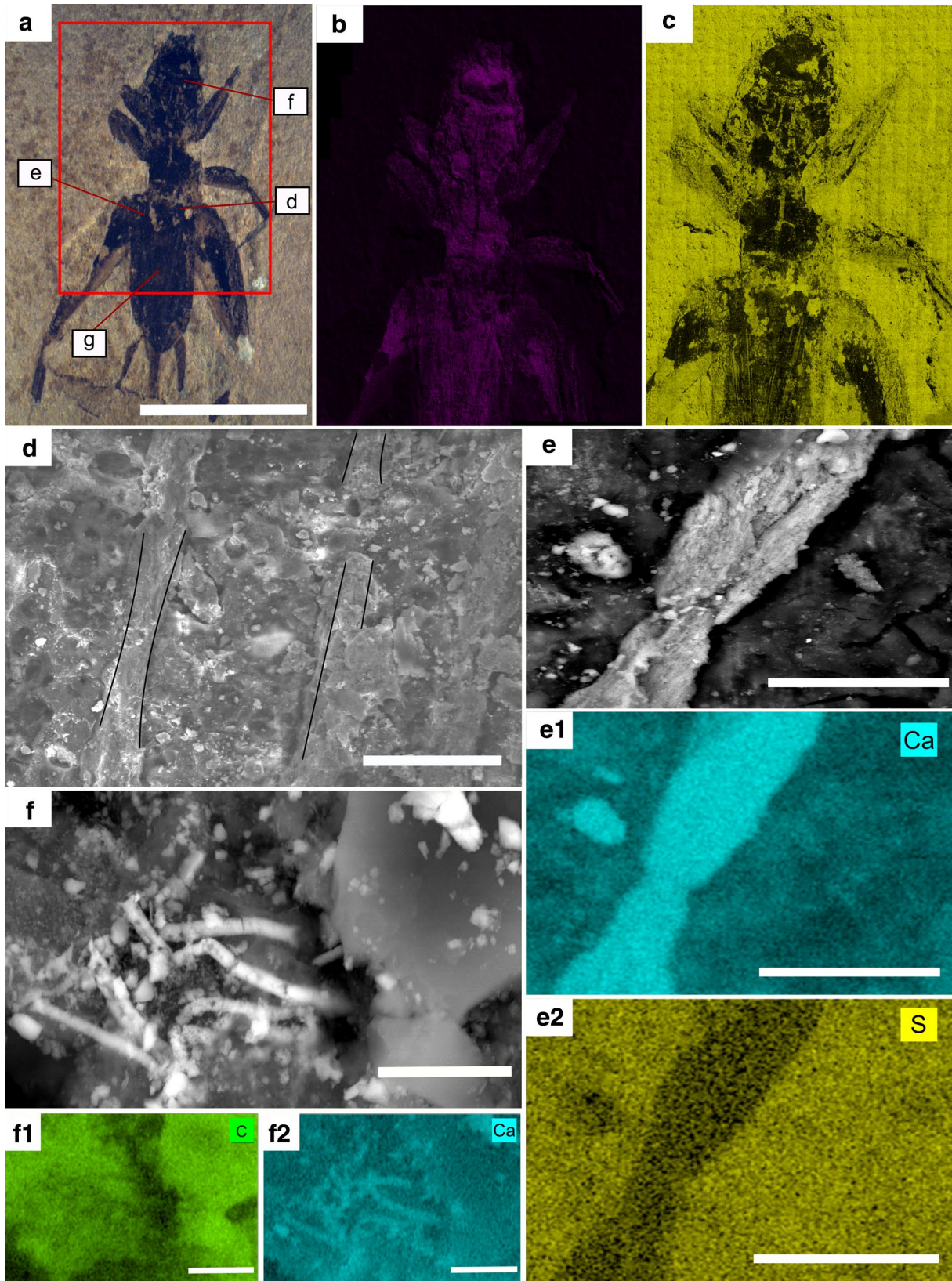


Fig. 2 SEM–EDS analyses of Crato Formation Ensifera from DL layers (a), light photomicrograph of LP/UFC CRT 2455, the areas analyzed shown by the red square. Scale bar=5 mm (b), large-field carbon elemental map (c), large-field calcium elemental map (d), scanning electron microscopy secondary electron image of parallel longitudinal veins. Scale bar=50 μm (e), details of the individual vein. Scale bar=25 μm (e1, e2) Ca and S maps, respectively, of the subfigure e. Scale bars=25 μm (f), calcified filaments covering the fossil. Scale bar=5 μm (f1, f2), C and Ca maps, respectively, of the subfigure f. Scale bars=5 μm

framework is organized in three major tectono-stratigraphic phases, called pre-rift, syn-rift, and post-rift (Ponte and Ponte Filho 1996; Assine 2007). The pre-rift phase is characterized by siliciclastic fluvial-lacustrine sediments deposited during the Late Jurassic. It is composed by Brejo Santo and Missão Velha Formations. The syn-rift phase developed in the Berriasian–Early Aptian, is fluvial and lacustrine siliciclastic sediments from the Abaiara Formation (Assine 2007). The post-rift phase starts with mixed siliciclastic–carbonate–evaporite successions (Santana Group) and finishes with entirely siliciclastic deposits (Araripe Group). The main fossiliferous unit, Crato Formation, evolved in the middle Santana Group during the Late Aptian–Early Albian.

The Crato Fm. comprises a 70 m-thick succession and is composed of metric-scale laminated carbonate units inter-layered with equally thick successions of green shales and fine-to-coarse sandstones (Assine et al. 2014; Santos et al. 2017). The lacustrine carbonate facies is made of micritic laminated limestones composed by calcite with low magnesium content (Catto et al. 2016). According to Martill et al. (2007), the presence of halite pseudomorphs in some levels suggests deposition under fluctuating salinity conditions. The origin of the Crato carbonates was attributed to chemical precipitation from the water column by Heimhofer et al. (2010), despite recently evidences of benthic microbial activity described by Catto et al. (2016) and Warren et al. (2017). According to Coimbra et al. (2002), the Crato Formation is part of the *Sergipea variverrucata* palynozone suggesting an Aptian age for the unit.

3 Materials and methods

3.1 Fossil material

The Ensifera fossils are deposited in the Scientific Palaeontological Collection of the Laboratório de Paleontologia (LP) at the Universidade Federal do Ceará (UFC), Brazil. The material analyzed in this paper was collected from Pedra Cariri quarry in Nova Olinda, Ceará State. The specimens were chosen according to color-type of calcareous matrix: the sample LP/UFC CRT 2455 belongs to DL; LP/UFC CRT 1822 to RL and LP/UFC CRT 122 to YL.

3.2 Large-field energy dispersive spectroscopy (EDS) and scanning electronic microscopy (SEM) analysis

The SEM–EDS analyses were performed in the Central Analítica at the Universidade Federal do Ceará (UFC). The large-field scan was carried out in a Quanta-450 electron microscope (FEI) with a field-emission gun (FEG) equipped with a gaseous analytical detector (GAD), 10 mm working distance and a X-ray detector (model 150, Oxford) for energy dispersive X-ray spectroscopy (EDS). Images were acquired at beam acceleration voltage of 20 kV, using a resolution of 1024 \times 884 pixels per image. With the aim to maintain the integrity of the samples for future analysis we avoid to use a thin layer of gold–palladium on the fossil. Thus, the fossil material was inserted into the microscope chamber without previous preparation. The analyses were done in a low vacuum to avoid sample charging. To generate the large-field images, an overlapping of marginal areas (a border which contains 20% of the image area) of adjacent images acquired independently after translations of the microscope stage along the x and y axes was performed. The images were processed and exported on AZtec software (version 3.0/Oxford).

3.3 Raman spectroscopy

The Raman spectra were obtained by a LabRAM HR (Horiba) spectrometer equipped with a liquid N₂-cooled CCD detector behind a 600 g/mm grating, using 785 nm laser radiation for excitation (\sim 2 mW at the sample surface). For the Raman images, the sample was placed on an x–y stage and scanned under the illumination of the laser using an objective Leica 50 \times with numerical aperture (NA) of 0.80 used to focus on the sample surface with a power of 1 mW and an integration time of 20 s. The laser power was set at \sim 1 mW on the sample. Each spectral segment and each sample was measured several times in different positions. No sample preparation was necessary to this kind of measurement.

4 Results

4.1 Ensifera from DL

The DL layers correspond to the clay-carbonate rhythmite facies (Neumann et al. 2003); they are characterized by detrital clay contents and pale/dark banding. The dark part is rich in continent-derived detrital grains/organic debris, and the pale laminae are dominated by calcite crystals. The DL layers are dominated by euhedral to subhedral calcite crystals varying between 2.1 and 4.6 μm . Within the cuticle the size of the crystals ranges from 3.1 to 11 μm and alveolar

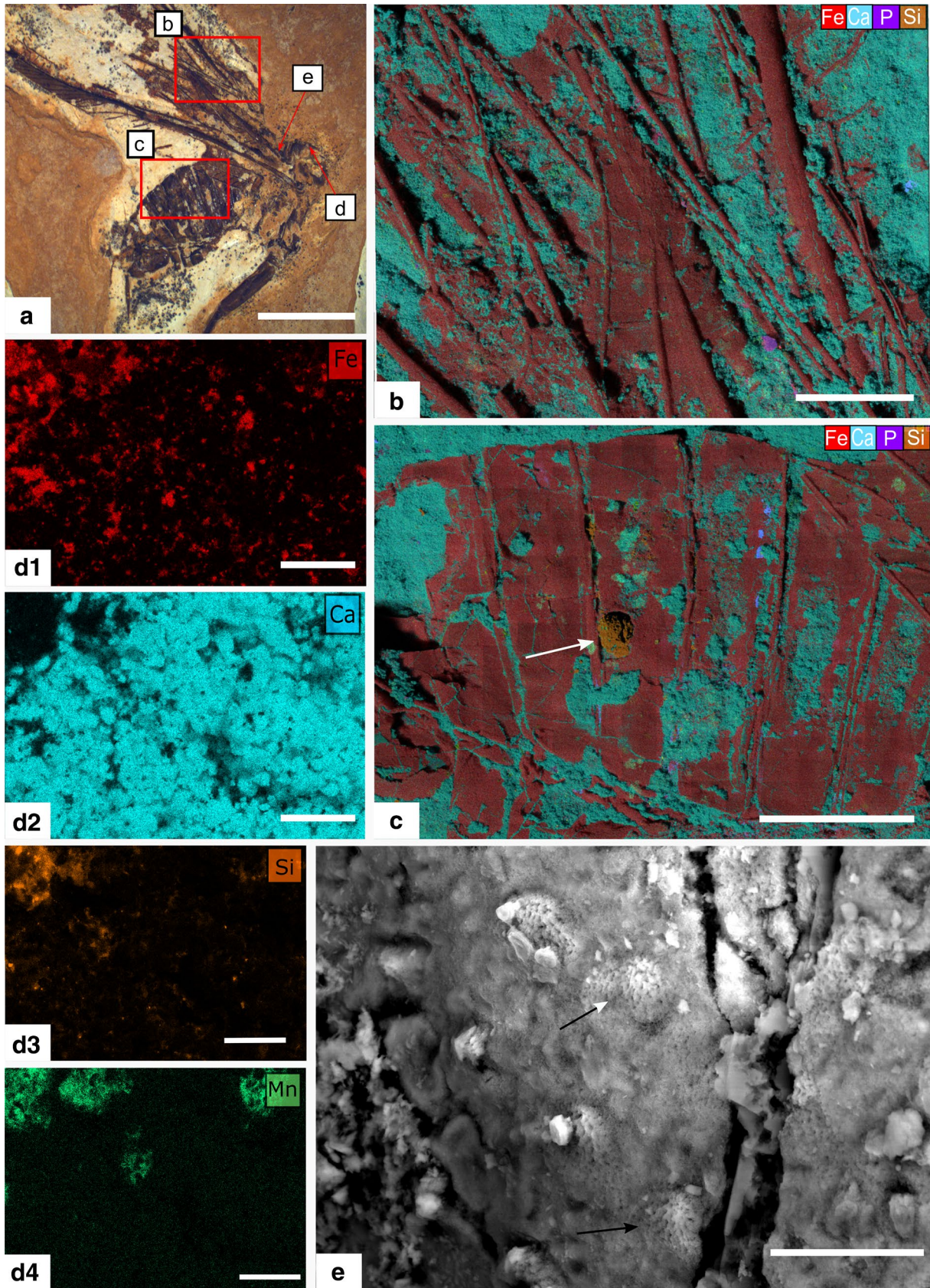


Fig. 3 SEM–EDS analyses of Crato Formation *Ensifera* from RL layers (a), light photomicrograph LP/UFC CRT 2288, the areas analyzed shown by red squares. Scale bar = 5 mm (b, c), large-Field-EDS maps of several elements distributed in the wing and abdomen, respectively. Scale bars = 2 mm (d1–d4), Fe, Ca, Si and Mn elemental maps of the head, respectively. Scale bars = 50 μm (e), scanning electron microscopy secondary electron image, revealing microfabric of the cuticle. Black arrow points to pyrite framboids. Scale bar = 4 μm

structures with spherical calcite are preserved as well. The SEM analyses from LP/UFC CRT 2455 reveal that the cuticle soft-tissue consists of a thick dark material without well-defined microfabrics often covered by calcite debris.

The secondary electron (SE) analyses reveal finer details hidden by the naked eye that resemble biogenic features, such as numerous fine long fibrous-like interconnected segments of LP/UFC CRT 2455 (Fig. 2d). We interpreted these structures as the major wing veins (Fig. 2e) (Chapman 1998).

In some parts, individual grains of micro-rhombohedral calcite associated with the presence of filaments varying from 2.0 to 3.6 μm in size (Fig. 2f) covering the fossil may have biological origin. The filaments indicate that rhombohedral calcite is product of biologically-induced precipitation by bacterial activity (Catto et al. 2016).

The concentrations of both elements C and Ca in the fossil LP/UFC CRT 2455 suggest that the C is distributed throughout the fossil (Fig. 2b). The richest areas in the C elemental map match with the fossil (Fig. 2b, c). EDS analyses reveal carbon, sulfur and phosphorus clearly correlated in the fossil outline and these elements are substantially reduced in the matrix. The low abundance of iron and manganese attest to the minimal weathering undergone by the sample (Supplementary material Table 1).

The Raman spectrum from LP/UFC CRT 2455 is unclear because Raman scattering was superimposed on an intense luminescence background. Increasing the acquisition time resulted in a corresponding increase in the overall spectral intensity, but no significant change in spectral shape was noted. Thus, it was not possible to acquire Raman spectra from the sample LP/UFC CRT 2455.

4.2 *Ensifera* from RL

We analyzed the specimen LP/UFC CRT 1822 (three-dimensionally preserved) in two regions: the wing (Fig. 3b) and the abdomen (Fig. 3c). The Secondary Electron analysis revealed that the rock matrix is composed of euhedral to subhedral rhombohedral calcite with diameters ranging mainly between 5 and 15 μm . The preservation fabric within LP/UFC CRT 1822 is dominated by small hollow crystals or cylindrical aggregates forming small clusters. The cuticle is also commonly arranged into hollow spherical or cylindrical aggregates that vary in size between 1 and 15 μm in

diameter; the hollow spheres often appear to be merged into larger globular clusters. The exoskeleton can display a weakly laminar arrangement. The cuticle cavities are filled with grains of approximately 1–2 μm . According to Barling et al. (2015) and Osés et al. (2016), this pattern seems to be the result of a precursor mineral. These authors have interpreted these minerals as pyrite framboids–pseudoframboids (Fig. 3e).

SEM–EDS analysis shows higher concentration of terrigenous elements, such as Si and Mn (Fig. 3d3, d4) in LP/UFC CRT 1822 than in the *Ensifera* from DL layers. Nodules composed of Si often appear inside the fossil (Fig. 3c). Large-Field electron scans also show that Fe-rich mineralization in fossil LP/UFC CRT 1822 is higher than in surrounding matrix (Fig. 3b, c). EDS analyses indicate the Fe-oxide-rich coatings have low abundance of sulfur; sulfur has probably been lost through diagenesis or weathering. We inferred that the loss of sulfur has occurred by weathering (Littke et al. 1991). The concentration of iron plus depleted-sulfur suggest that the pyrite framboids are early diagenetic and underwent oxidation later. Besides that, dissolution cavities in cuticle, described by Osés et al. (2016), reinforces the oxidation hypothesis.

Raman data reinforces the hypothesis of Fe sulfide phase's oxidation during surface weathering as discussed below. According to Goldhaber (1983), pyrite oxidation begins through a direct attachment of an O_2 molecule to the surface of pyrite. Singer and Stumm (1970) observed Fe^{3+} as the main oxidizing complex of pyrite at acidic pH, while O_2 is expected to be the direct pyrite oxidant at neutral and alkaline pH due to the low solubility of Fe^{3+} . However, Moses et al. (1987) and Moses and Herman (1991) concluded that Fe^{3+} may be a very effective pyrite oxidant even at circumneutral pH. Fe^{3+} is evidently the preferred reactant, but the reaction could only be sustained in the presence of O_2 because the reaction mechanism involves electron transfer from adsorbed Fe^{2+} to O_2 followed by electron transfer from pyrite to the resulting adsorbed Fe^{3+} . In this point, it is worth noting that goethite presents in the Raman spectrum peaks at 225, 297 and 393 cm^{-1} , but the latter two bands have higher intensities. As a consequence, the defined peaks at 295 and 393 cm^{-1} in the Raman spectrum (Fig. 4) can be attributed to the goethite (Perardi et al. 2000; Li and Hihara 2015). Thus, Raman spectrum revealed goethite as the main identified phase in the LP/UFC CRT 1822.

4.3 *Ensifera* from YL

The YL layers correspond to the laminated limestone facies of Neumann et al. (2003). Fossils of this layer are often three-dimension and uncompact and sometimes display iridescence (Barling et al. 2015). The YL layers are dominated by sub-spherical calcite crystals between 5 and 8 μm

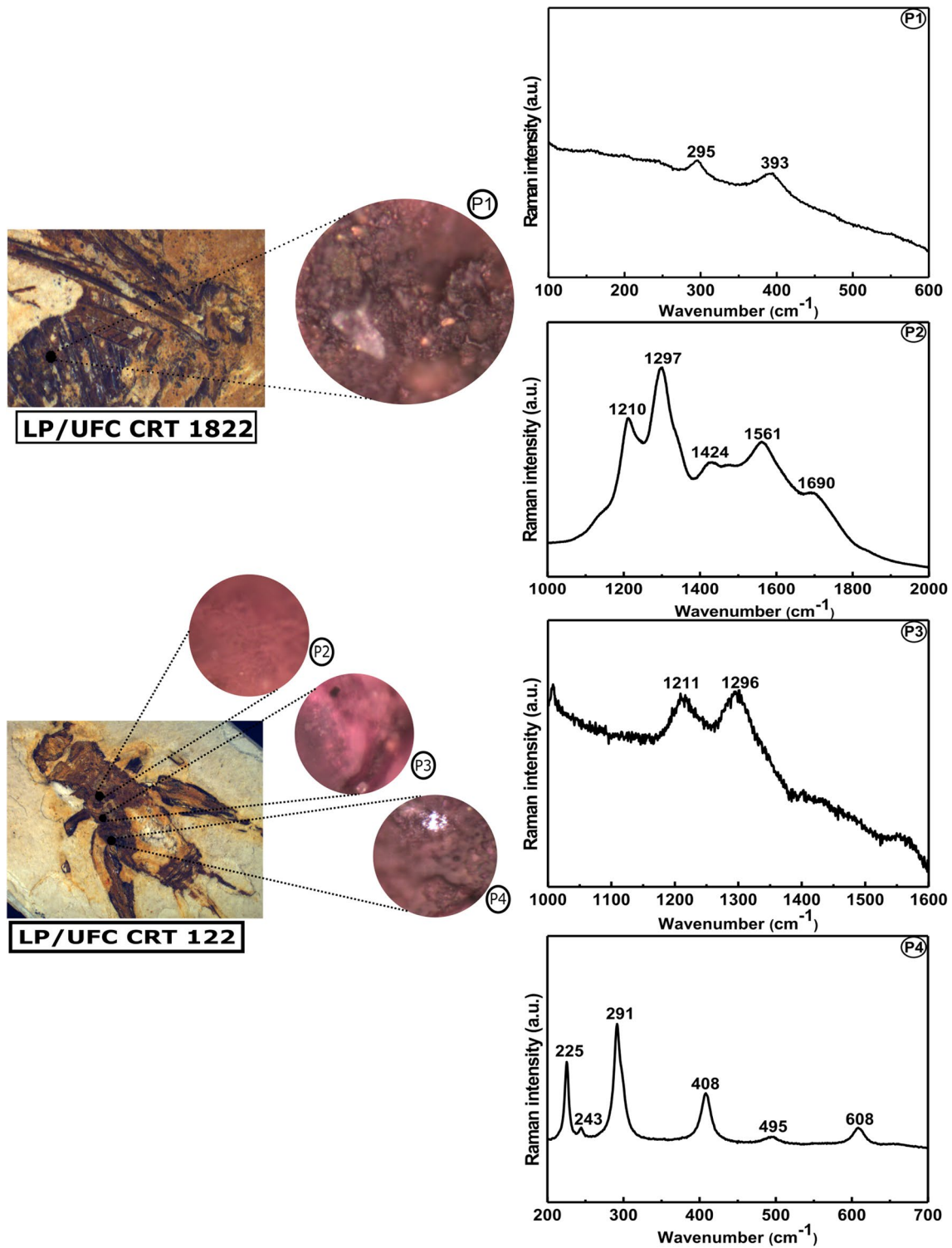


Fig. 4 Raman spectra of cuticle from LP/UFC CRT 1822 showing peaks at 295 and 393 cm^{-1} associated with goethite (p1). Raman spectra of different points (p2, p3 and p4) in LP/UFC CRT 122. p2,

p3 presents peaks in the wavenumber region 1200–1700 cm^{-1} ; p4 shows peaks in the wavenumber region 200–610 cm^{-1}

in diameter. We analyzed the specimen LP/UFC CRT 122 in three regions: head, thorax and abdomen (Fig. 5). LP/UFC CRT 122 presents a greater diversity of structures/

ultrastructures than the samples from the DL and RL layers. The Secondary Electron analyses revealed that the fossil cuticle is preserved by spherical to sub-spherical crystals

5–4 μm in diameter (Fig. 5e). The sample is composed of brownish minerals containing Fe-oxides. The Fe-oxide-rich grains in the specimen were arranged into two types: microspherules and framboids. The microspherules vary in size between 0.3 and 0.4 μm in diameter (Fig. 5f) and occur preferentially within the cuticle. Microspherules are often regular in shape and size. The framboids (Fig. 5h) are rarer than the microspherules and occur irregularly in wrinkled areas in the abdomen, varying in size from 2 to 4 μm . Other portions of the sample are preserved as dark-colored films (Fig. 5g) composed predominantly of carbonaceous material (Fig. 6).

Large-Field scans on the specimen LP/UFC CRT 122 revealed higher iron concentration within the outline of the organism instead of the matrix (Fig. 5b–d), indicating the Fe element equally distributed in the fossil. The specimen is slightly weathered. EDS analyses suggest that the microspherules and framboids are now composed of Fe-oxides/hydroxides. The original spherical morphology of framboidal Fe-rich diagenetic minerals as well as the microspherules were probably both precipitated as pyrite.

The C and Fe concentrations are higher in the fossil than in the carbonate matrix. EDS analyses showed occurrence of Si and Al (Supplementary material Table 1) in low amount which can be attributed to siliciclastic inputs (Neumann et al. 2003; Heimhofer and Martill 2007; Heimhofer et al. 2010; Santos et al. 2017). The presence of sulfur is substantially reduced when compared to *Ensifera* from the DL layers, and does not match the fossil outline.

LP/UFC CRT 122 retains preservational details that can be found in LP/UFC CRT 2455 and LP/UFC CRT 1822, described above. This means that the *Ensifera* from YL layer could be exposed to processes that occurred in both DL and RL layers.

The Raman spectra of LP/UFC CRT 122 are the most complex spectra among the sample fossils (Fig. 4). The heterogeneous character of the sample is shown through different peaks recorded at various positions. Signals were observed occurring mainly in two spectral regions: 200–610 cm^{-1} and 1200–1700 cm^{-1} . Figure 4, p2 shows a spectral region where it is possible to observe bands related to stretching vibrations of carbon in general ways. For example, just to cite a few, carbon with a certain structural disorder can present peaks at 1350 and 1580 cm^{-1} , while graphite presents an internal band at 1580 cm^{-1} (Ferrari and Robertson 2001). Regarding the spectrum shown in p1, an important band around 1210 cm^{-1} was assigned as defect band D4 associated with disordered crystal structure. This band is usually observed as a lower energy shoulder of D1 due to sp^2 – sp^3 bonds or vibrations from single and double bond carbons (Sadezky et al. 2005; Herdman et al. 2011). Jehlička et al. (2003) reported D4 defect band in solid bitumen. Sadezky et al. (2005) also observed similar band in

glassy carbon. The band around 1297 cm^{-1} was associated with CH_2 scissors modes (Edwards et al. 2007). The peak at 1424 cm^{-1} can be associated with the antisymmetric stretching of CO_3^{2-} (Freire et al. 2014). We observe band around 1561 cm^{-1} which can be assigned to G bands (Ferrari and Robertson 2001; Alencar et al. 2015). Truică et al. (2014) attributed the band at 1690 cm^{-1} to the C–O bond stretching. In summary, this region presents a series of bands that are associated with vibrations involving the carbon atom.

The spectrum presented in Fig. 4.p3 indicates high luminescence, showing the difficulty of obtaining acceptable signals along the sample. However, it is possible to observe two huge bands. Bands at 1211 and 1296 cm^{-1} correspond to defect band D4 and CH_2 bend, respectively. In the present study, some of our Raman spectra (Fig. 4, p2–p3) clearly showed the presence of carbonaceous material in the LP/UFC CRT 122. On the other hand, we have observed the presence of bands that can be associated with late diagenetic minerals. The spectrum showed bands at 225, 243, 291, 408, 495 and 608 cm^{-1} (Fig. 4, p4), corresponding to the mineral hematite Shim and Duffy (2002). Bands related to pyrite (e.g., 343, 350, 376, 379, 430 cm^{-1}) (Vogt et al. 1983; Freire et al. 2013) were not recorded in any analyzed area. Bands associated with carbonaceous material occur in the dark smooth areas of the fossil, while characteristic vibrational modes of hematite increase in the light wrinkled regions.

5 Discussion

According to Martill and Heimhofer (2007), the Crato Formation had essential conditions for preservation, based on the presence of halite pseudomorphs (oxygen solubility in water is known to decrease with increasing salinity) and absence of sediment mixed by bioturbation, indicating hypersalinity and anoxic conditions. However, anoxia alone was not sufficient to retard the decay of tissue. In fact, insect tissues can survive for over a year in oxygenated conditions if undisturbed (Martínez-Delclòs and Martinell 1993). Only under reducing conditions, tissue decay is strongly retarded, remaining intact for long period until mineralization occurs (Butler et al. 2015). The notion of mineralization associated with biofilms suggests that internal biofilms are the precursors to exceptional preservation through the mineral replication of soft-tissue anatomy, as supported by previous studies (Sagemann et al. 1990; Briggs 2003; Raff et al. 2008; Briggs and McMahon 2006; Laflamme et al. 2011; Butler et al. 2015). They may trap the carcasses forming an enclosed system around each fossil (Briggs 2003). Wang et al. (2012) reported pyrite halos around insect fossils suggesting the presence of reducing microenvironments facilitated by microbial mats. Therefore, the mineralization of soft-tissues requires a precise balance between rate of decay

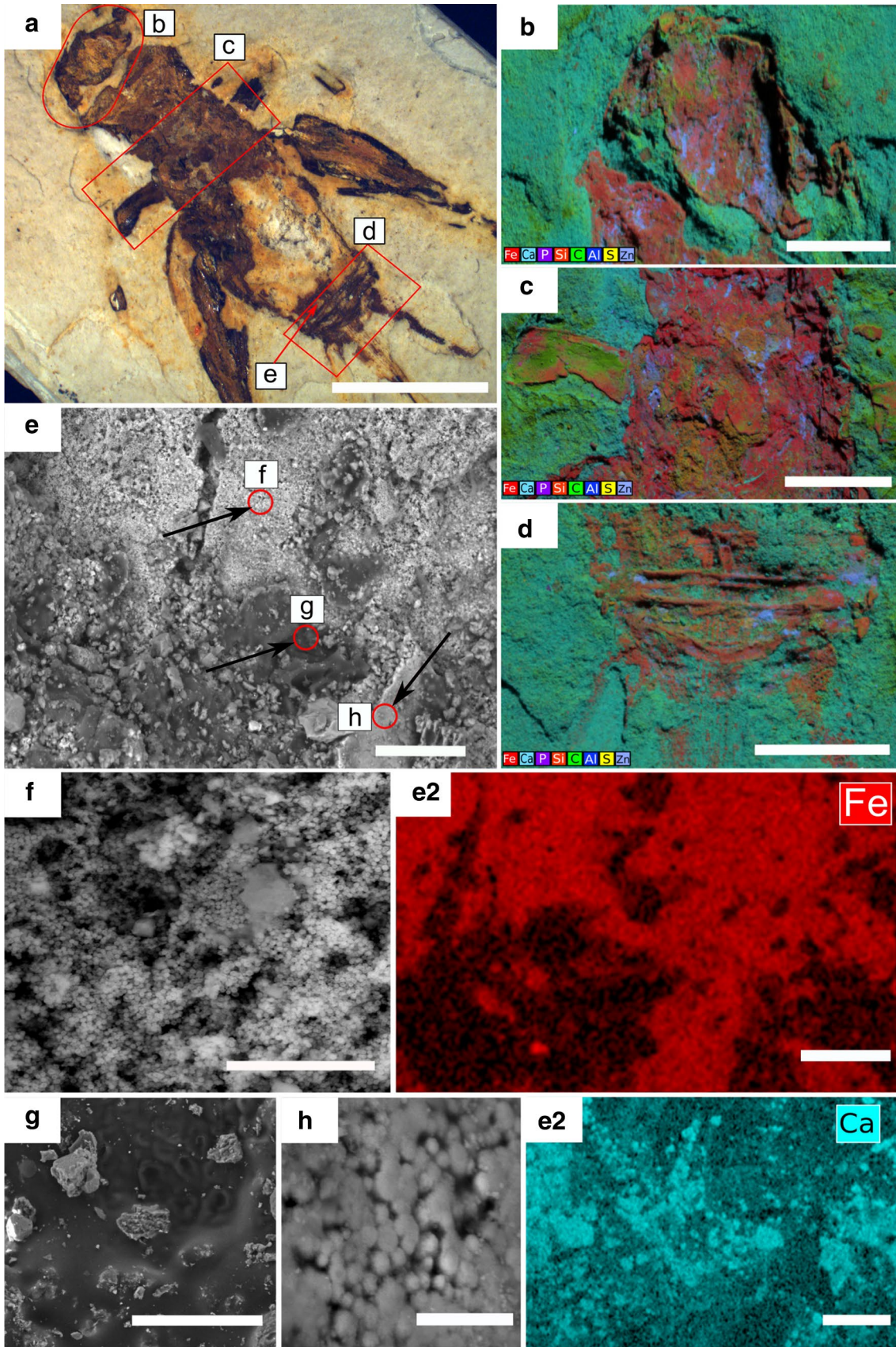


Fig. 5 SEM-EDS analyses of Crato Formation Ensifera from YL layers (a), light photomicrograph of LP/UFC CRT 122, the areas analyzed shown by red squares. Scale bar=4 mm (b–d), large-Field-EDS maps display elemental overlap in the head, thorax and abdomen, respectively. Scale bars=2 mm (e), scanning electron microscopy secondary electron image for abdomen mineral characterization. Note three textural domains. Black arrows indicate microspherules grains, framboid minerals and carbonaceous materials. Scale bar=50 μm (f), higher magnification scanning electron micrograph of e, showing microspherules. Scale bar=10 μm (g), detail of e showing dark material without well-defined microfabric. Scale bar=10 μm (h), higher magnification image of e, highlighting framboidal pyrite. Scale bar=10 μm (e1, e2), Fe and Ca, respectively, elemental maps of e. Scale bars=50 μm

and diffusion of mineral ions in the anaerobic bacterial respiration zone (Bacterial Sulfate Reduction zone—BSR zone) within the sediment. The sediment column typically consists of an aerobic respiration zone in the water–sediment interface, followed by an anaerobic zone with nitrate, manganese and iron reduction, then the sulphidic zone, and finally the methanogenesis zone at depth (Schiffbauer et al. 2014).

The specimen LP/UFC CRT 2455 from DL is preserved by black, amorphous and homogeneous material. In this sample, EDS elemental maps clearly show strong localization of carbon within the body outline. The amorphous character and absence of distinctive ultrastructure in fossil arthropod cuticles is consistent with polymerization of epicuticular lipids within the cuticle (Stankiewicz et al. 1997). The absence of ultrastructure may be due to degradation of cuticular waxes and tissue lipids during diagenesis (Stankiewicz et al. 1997, 1998). The distinctive gross morphological preservation is here interpreted as kerogen, based on the interpretation of Osés et al. (2017), who have proposed a preservation model for *Dastilbe crandalli* from the Crato Formation. Osés et al. (2017) revealed that the fish soft-tissues preservation were controlled by distinct sedimentation rates in two different facies, which fish carcass deposited in each of these facies underwent different residence times in sulphate-reduction and methanogenesis zones. Thus, our results strongly match with the model proposed by Osés et al. (2017).

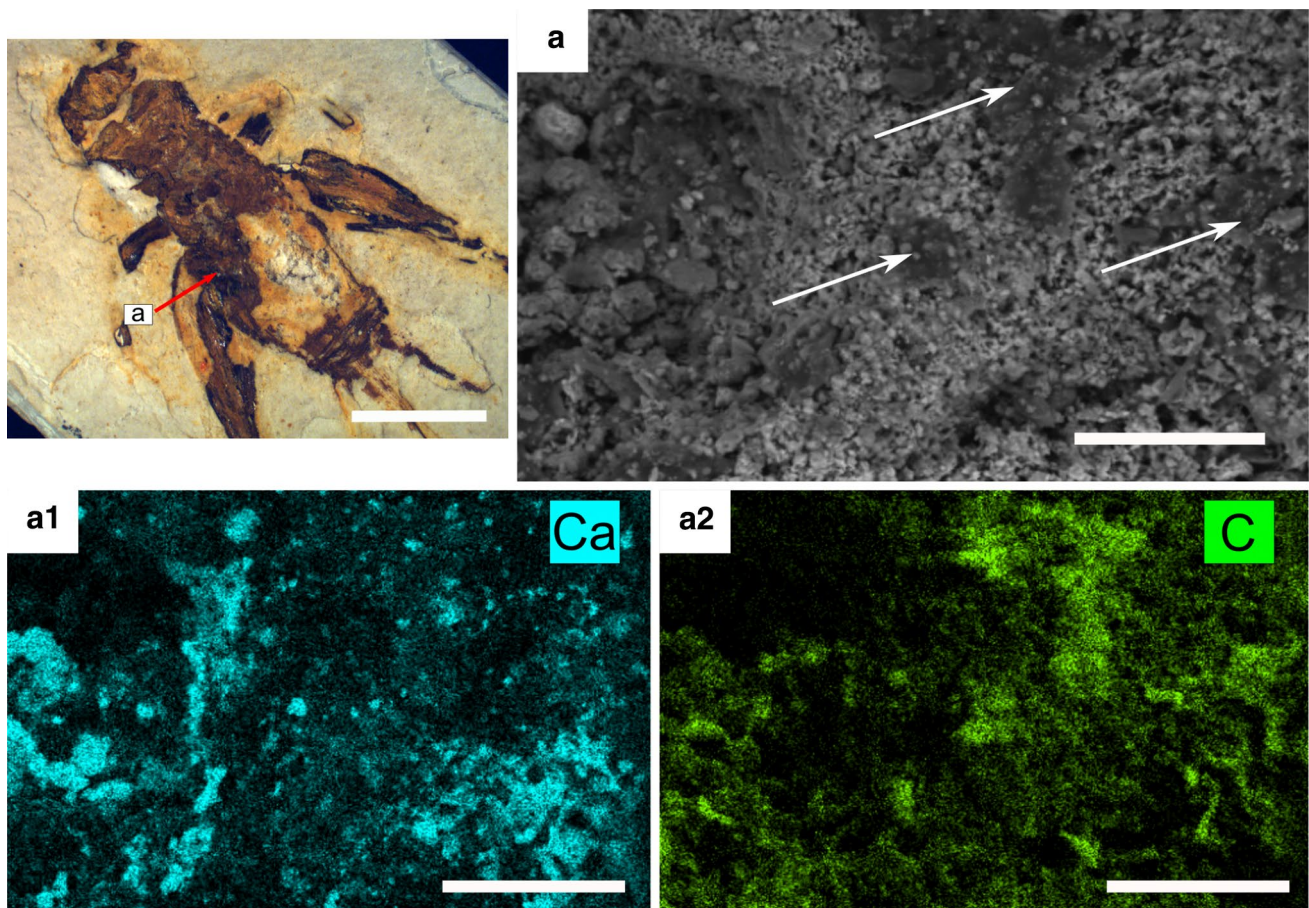


Fig. 6 SEM-EDS analyses of the basal coxa from LP/UFC CRT 122 (a), scanning electron microscopy secondary electron micrograph, dark material is indicated by white arrows. Scales bar=50 μm (a1, a2), Ca and C elemental map of a, respectively. Scales bars=50 μm

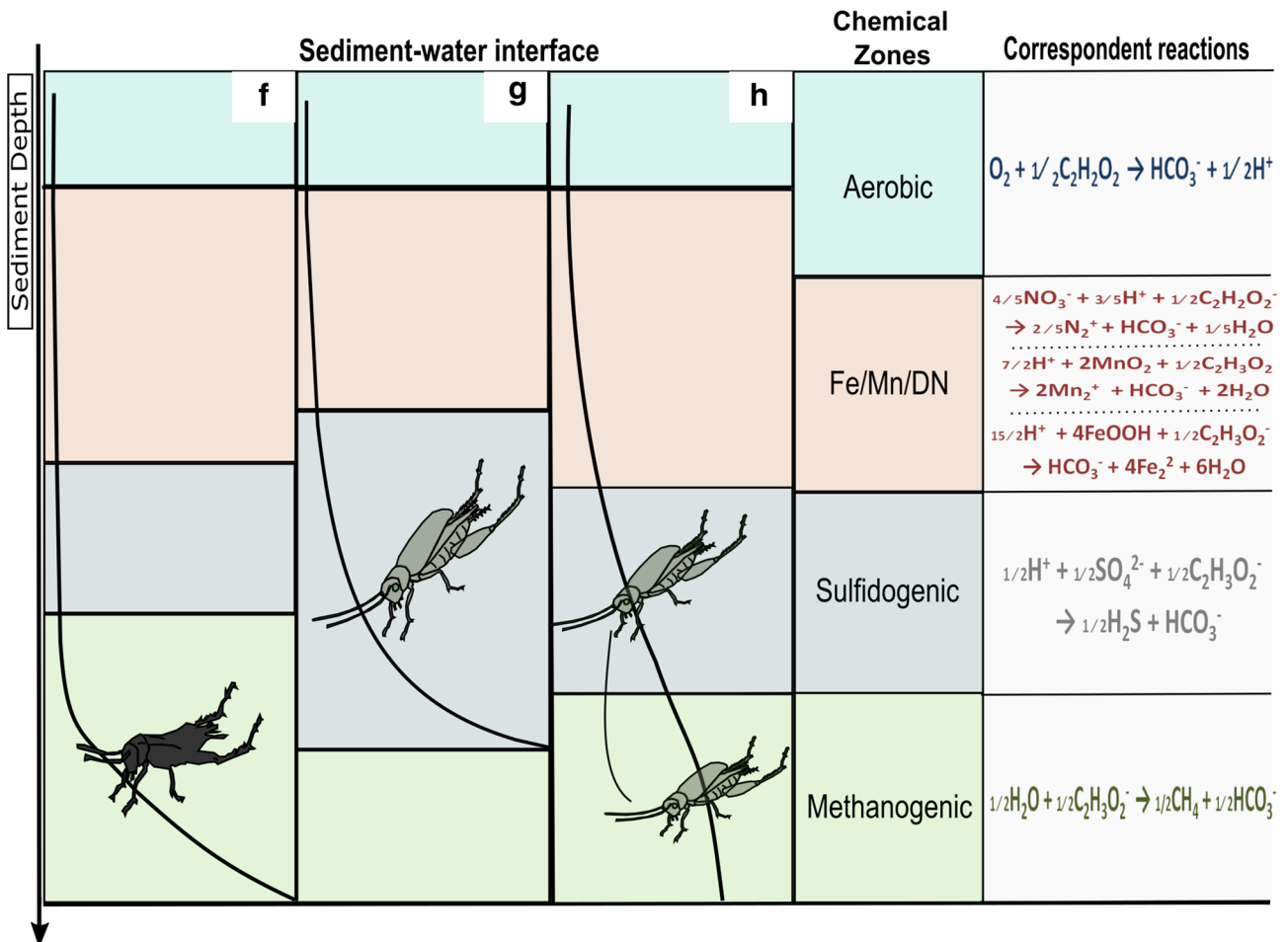
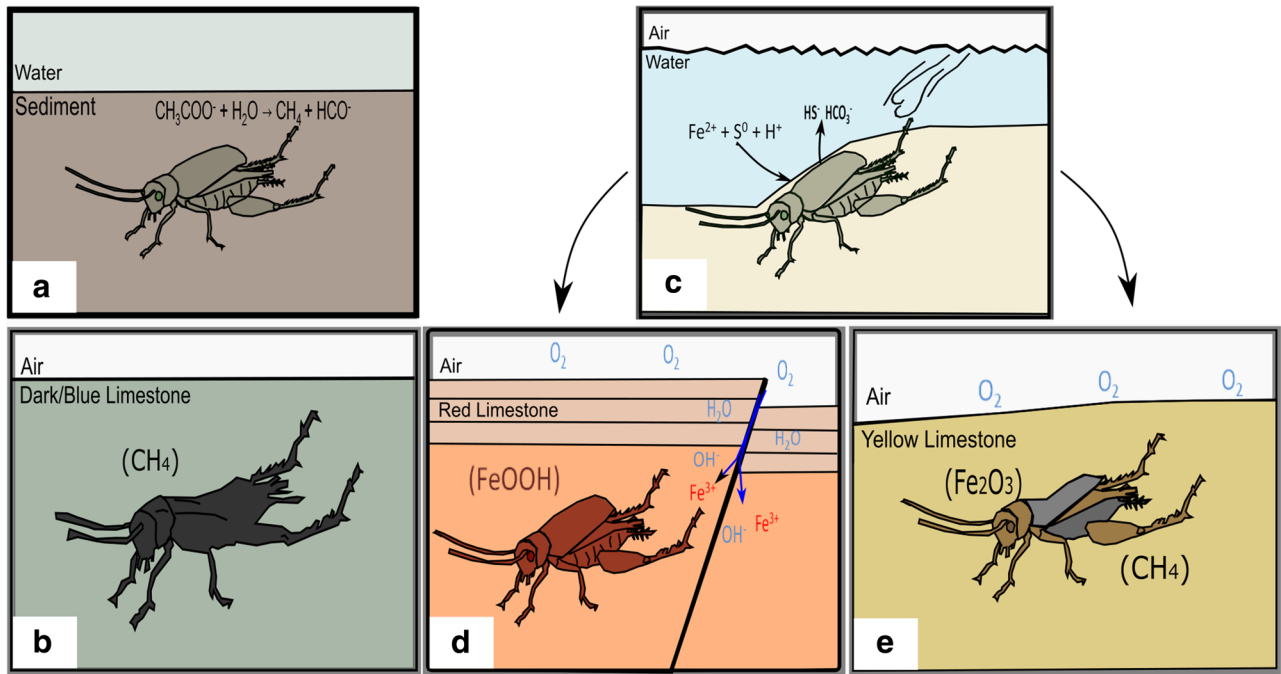


Fig. 7 Taphonomic pathways of the Crato Formation *Ensifera* (a–e), upper figure shows the specimens during early–late diagenesis (a), shows fossil from DL layers in the methanic zone (b), specimen from DL layers preserved by complete kerogenization (c), represents early preservation stages of *Ensifera* from RL and YL layers in the BSR zone (d), indicates the post-diagenetic alteration undergone by the fossil of the RL layers (e), shows specimen from YL layers with admixed preservation mode pyrite-carbonaceous material. The lower diagram shows the fossils located in the correspondent simplified sedimentary microbial zone. Black diagonal lines track the position of the decaying organisms in the sediment column. Curves from left to right represent an increase in the residence time of the fossil within the geochemical zone. Microbial respiration process zonation and correspondent reactions based on Canfield and Thamdrup (2009). Sediment depth is represented by vertical black arrow (f), corresponding diagram shows that in DL the fossils spent more time in the methanic zone, hence yielding complete kerogenization (g), diagram shows initial rapid event deposition combined with thick sulfate reduction zone making pervasive pyritization possible in RL (h), diagram shows a reduction of residence time in the BSR zone thickness, leading to earlier depletion of pyritization and onset of kerogenization, in the YL. The hypothetical diagram style is based on Cai et al. (2012); Schiffbauer et al. (2014); Osés et al. (2016) and Osés et al. (2017)

The anoxic bottom water body of Crato paleolake prevented the organic matter of the heterotrophic bacteria degradation. Indeed, chitin contains a complex set of biomolecules such as polysaccharide and glycolipids. This complexation may induce greater resistance to degradation (Vandenbroucke and Largeau 2007). Once in the methanogenesis zone (Fig. 7a), the carcass degradation is mostly limited to labile tissues, such that only the recalcitrant tissues become kerogen (Fig. 7b) (Schiffbauer et al. 2014). According to Osés et al. (2017) hypothesis, the varied cement and clay contents in DL contributed to reduce the thickness of sulphate percolation zone, as a consequence, facilitating the carcasses displacement through the zones, even in low sedimentation rates (Fig. 7f). Moreover, the higher organic matter accumulation in the DL favoured the iron/sulphate concentration scattered in the carbonate also prevented LP/UFC CRT 2455 of being mineralized.

The fossil LP/UFC CRT 1822 from RL layers is mainly composed of iron oxide/hydroxide spherical grains, sometimes constituting aggregates, which we interpret to be originally preserved by framboidal pyrite as previously described by de Delgado et al. (2014) and Osés et al. (2016). The pervasive pyritization undergone by LP/UFC CRT 1822 can provide insights into early diagenetic conditions required by this taphonomic style. According to Raiswell et al. (1993), the diffusion–precipitation model of pyritization is controlled by located decay of organic matter and reactive iron within Bacterial Sulfate Reduction (BSR), where the carcass is the sulfide source (Fig. 7c). Briefly, the precipitation of pyrite can occur as $\text{Fe}^{2+} + \text{S}^0 + \text{HS}^- \rightarrow \text{FeS}_2 + \text{H}^+$, presuming an estimated ratio of reservoir concentrations (C^0) of sulfur to iron, ($C_{\text{S}}^0 : C_{\text{Fe}}^0 < 0.1$) for localized pyrite formation at

the site of decay (Raiswell et al. 1993). In the other words, reactive iron [Fe^{2+}] must be greater than dominant dissolved sulfite [HS^-] to induce pyrite precipitation around the carcass. Although pyrite precipitation can certainly occur where sulfide is higher than ferrous iron, its nucleation on the carcass is not expected.

The calcareous facies of the Araripe Paleolake are commonly poor in total organic carbon (Catto et al. 2016). The main source of iron consist in freshwater pulses (Catto et al. 2016; Santos et al. 2017), probably as Fe^{3+} that under anaerobic respiration is reduced to Fe^{2+} , thus driving mineralization. The low values of organic matter made possible the fossil pyritization in the Crato Formation (Osés et al. 2017), thus, few decay sites in the BSR zone allowed the sulfite from sulfate reduction to be fixed by Fe^{2+} into pyrite and concentrated in carcasses and not diffused through the sediment.

The LP/UFC CRT 1822 is completely pyrite-replaced, which suggests that initial pyrite mineralization must have occurred rapidly and entirely in the BSR zone (Fig. 7g). The low organic matter and terrigenous content potentially favoured the pervasive pyritization. The specimen was quickly placed below the aerobic zone; otherwise, its three-dimensional structural integrity would have been affected.

The defined peaks at 295 and 393 cm^{-1} in the Raman spectrum are attributed to goethite. This fossil preservation style strongly suggests the specimen has been oxidized in situ over a prolonged period (Menon and Martill 2007; Barling et al. 2015), as also evidenced by the reddish color of the RL layers. In this paper, we concluded that the oxidation of specimens is closely associated with the limestone weathering process, which in turn is related to the topographic inversion of the Araripe Basin. Morais Neto et al. (2005–2006) identified two exhumation events in this basin; the first event probably began during the Upper Cretaceous, and the second one occurred during the Oligocene or later. Therefore, uplift of the Araripe plateau promoted the establishment of fractures/faults facilitating the underground percolation of meteoric waters, hence carrying ions leading to oxide/hydroxide formation from a precursor pyrite mineral (Fig. 7d).

The specimen LP/UFC CRT 122 from YL layers is preserved three-dimensionally through incomplete pyritization. Elemental maps indicate a prevalence of iron and also showed positive carbon concentration in the fossil. The pyritization is dominated by precipitation of framboids and abundant micrometric crystals (microspherules), as observed in some abdomen portions (Fig. 5f). The distinct sizes of crystals replacing LP/UFC CRT 122 suggest different nucleation rates. Thus, the smallest framboids are formed under conditions favourable to rapid nucleation (Butler and Rickard 2000) controlled by high decay sites. In the other words, the localized distribution of crystals

indicate that the organic surface likely plays a role in directing the onset of nucleation, during the earliest stages of microbially induced degradation (Butler et al. 2015).

The Raman spectral data demonstrate a strong contrast on the preservation mode of LP/UFC CRT 122 (Fig. 4). The intense bands around 1200–1700 cm^{-1} suggest the presence of carbonaceous material, probably invertebrate cuticle source, and bands around 200–610 cm^{-1} , indicate hematite (resulting from the pyrite oxidation). A possible explanation for the difference noted in the spectroscopic results could be attributed to primary microbial influence in both BSR and methanogenesis zones (Fig. 7h).

The thickness of the BSR zone is controlled by availability of organic carbon, sulfate and reactive iron in the sediment column. Incomplete pyritization is also facilitated by organic matter available, anoxic environment, reactive iron, low bioturbation and rapid placement in the BSR zone (Cai et al. 2012; Schiffbauer and Laflamme 2012; Schiffbauer et al. 2014). However, some required chemical component should be restricted and, consequently, the pyritization in the BSR zone should be prematurely depleted. As such, some possible approaches can be hypothesized, for example, the extent of the BSR zone can be reduced by faster consumption of diffusive sulfate, exhaustion of organic material and slow sedimentation rate may influence the availability of reactive iron. Alternatively, a high sedimentation rate could quickly transport the carcass from BSR zone to methanogenesis zone (it is unlikely for Crato Fm.), or even the earlier exhaustion of reactive iron could make the pyritization process incomplete (it is likely for Crato Fm.). Therefore, pervasive and incomplete pyritization can be controlled by how much time the carcass spends within the BSR zone (Schiffbauer et al. 2014). Thus, the admixed preservation mode of specimen from the YL (Fig. 7e) suggests a short residence time in the BSR zone and subsequent interaction with the methanogenesis zone.

6 Conclusions

The Crato Formation Ensifera fossils analyzed are extremely well preserved. SEM–EDS and Raman spectroscopy techniques exhibited at least two main taphonomic pathways: Kerogenized and Pyritized processes. Scanning electron microscopy analyses revealed that the fossil from DL consist of opaque, amorphous, thick, dark material without well-defined microfabric throughout the body. The fossil from RL exhibits microfibrils dominated by sub-spherical to spherical grains. The hollow spheres often appear to be merged into larger globular clusters. Sometimes, the cuticle cavities are filled with hollow crystals of calcite. Ensifera from YL displays mineral composition similar to RL and DL, including microspherulites and thick hard dark material, which

suggests an intermediate process between the two models mentioned above. These different preservation modes can be explained by the amount of time the carcass stayed within the methanogenesis and BSR zones. Kerogenized fossils were more rapidly buried in the methanogenesis zone. In contrast, the pyritized fossils spent more time in the BSR zone. Therefore, the taphonomic model for fish preservation of Osés et al. (2017) can be extended to insect preservation in the Crato Formation. In this context, the Crato Fm. presents a peculiar scenario to understand the taphonomic bias that controls two different preservation pathways within the same geological setting. Moreover, the three-dimensionality and framboidal pyrite in RL and YL fossils constitute evidence that pyritization occurred earlier in the taphonomic process. The Raman data also show that the fossils from RL and YL were later affected by slow oxidation of iron-sulphide phases during a subsequent event. Probably, the oxidation took place due to uplift of Araripe Basin from the Oligocene until recently. Indeed, the exceptional quality of fossils insects from Crato limestone *Lagerstätte* was directly influenced by a combination of different processes.

Acknowledgements We would like to acknowledge Laboratório de Paleontologia from Universidade Federal do Ceará for donat insect samples. We gratefully thank João Victor Serra Nunes and Marlos de Medeiros Chaves from Central Analítica-UFC for their assistance for SEM micrographs of insects. We thank Laboratório de Espectroscopia Vibracional e Microscopia (LEVM), Physical Department-UFC, for Raman analyses. Particular thanks to Dr. Wellington Ferreira da Silva Filho from Geology Department-UFC for his assistance with field-work and always encouraging our work on the Crato Formation. This study was financed in part by the Coordenação de Aperfeiçoamento de Pessoal de Nível Superior—Brasil (CAPES)—Finance Code 001. We acknowledge CAPES (process 88882.454892/2019-01) for FIB scholarship. JHS acknowledges the support from the MCTI/CNPQ/Universal No. 014/2015. JHS also thanks FUNCAP for the support granted through project B.P.I No 03/2018.

Compliance with ethical standards

Conflict of interest None.

References

- Alencar, W. J., Santos, E. P., Cisneros, J. C., Silva, J. H., Freire, P. T. C., & Viana, B. C. (2015). Spectroscopic analysis and X-ray diffraction of trunk fossils from the Parnaíba Basin, Northeast Brazil. *Spectrochimica Acta A*, *135*, 1052–1058.
- Anderson, E. P., & Smith, D. M. (2017). The same picture through different lenses: Quantifying the effects of two preservation pathways on Green River Formation insects. *Paleobiology*, *43*(2), 224–247.
- Assine, M. L. (2007). Bacia do Araripe. *Boletim de Geociências da Petrobras*, *15*(2), 371–389.
- Assine, M. L., Perinotto, J. A. J., Neumann, V. H., Custódio, M. A., Varejão, F. G., & Mescolotti, P. C. (2014). Sequências Depositionais do Andar Alagoas (Aptiano superior) da Bacia do Araripe,

- Nordeste do Brasil. *Boletim de Geociências da Petrobras*, 22(1), 3–28.
- Barling, N., Martill, D. M., Heads, S. W., & Gallien, F. (2015). High fidelity preservation of fossil insects from the Crato Formation (Lower Cretaceous) of Brazil. *Cretaceous Research*, 52(B), 605–622.
- Briggs, D. E. G. (2003). The role of decay and mineralization in the preservation of soft-bodied fossils. *Annual Review of Earth and Planetary Sciences*, 31, 275–301.
- Briggs, D. E. G., & McMahon, S. (2006). The role of experiments in investigating the taphonomy of exceptional preservation. *Palaeontology*, 59, 1–11.
- Butler, A. D., Cunningham, J. A., Budd, G. E., & Donoghue, P. C. (2015). Experimental taphonomy of *Artemia* reveals the role of endogenous microbes in mediating decay and fossilization. *Proceedings of the Royal Society B*, 282, 1–10.
- Butler, I. B., & Rickard, D. (2000). Framboidal pyrite formation via the oxidation of iron (II) monosulphide by hydrogen sulphide. *Geochimica et Cosmochimica Acta*, 64, 2665–2672.
- Cabral, F. A. A., Silveira, A. C., Ramos, G. M. S., Miranda, T. S., Barbosa, J. A., & Neumann, V. H. (2019). Microfacies and diagenetic evolution of the limestones of the upper part of the Crato Formation, Araripe Basin, northeastern Brazil. *Brazilian Journal of Geology*, 49(1), e20180097.
- Cai, Y., Schiffbauer, J. D., Hua, H., & Xiao, S. (2012). Preservational modes in the Ediacaran Gaojiashan Lagerstätte: pyritization, aluminosilicification, and carbonaceous compression. *Palaeogeography, Palaeoclimatology, Palaeoecology*, 326–328, 109–117.
- Canfield, D. E., & Thamdrup, B. (2009). Towards a consistent classification scheme for geochemical environments, or, why we wish the term ‘suboxic’ would go away. *Geobiology*, 7, 385–392.
- Catto, B., Jahnert, R. J., Warren, L. V., Varejão, F. G., & Assine, M. L. (2016). The microbial nature of laminated limestones: Lessons from the Upper Aptian, Araripe Basin, Brazil. *Sedimentary Geology*, 341, 304–315.
- Chapman, R. F. (1998). *The insects: Structure and function*. Cambridge: Cambridge University Press.
- Coimbra, J. C., Arai, M., & Carreno, A. L. (2002). Biostratigraphy of Lower Cretaceous microfossils from the Araripe Basin, northeastern Brazil. *Geobios*, 35, 687–698.
- de Delgado, A. O., Buck, P. V., Osés, G. L., Ghilardi, R. P., Rangel, E. C., & Pacheco, M. L. (2014). Paleometry: A brand new area in Brazilian science. *Materials Research*, 17, 1434–1441.
- Dias, J. J., & Carvalho, I. S. (2020). Remarkable fossil crickets preservation from Crato Formation (Aptian, Araripe Basin), a Lagerstätten from Brazil. *Journal of South American Earth Sciences*, 98, 102443.
- Edwards, H. G. M., Farwell, D. W., & Villar, S. E. J. (2007). Raman microspectroscopic studies of amber resins with insect inclusions. *Spectrochimica Acta A*, 68, 1089–1095.
- Ferrari, A. C., & Robertson, J. (2001). Resonant Raman spectroscopy of disordered, amorphous, and diamond like carbon. *Physical Review*, 64, 075414-13.
- Forchielli, A., Steiner, M., Kasbohm, J., Hu, S., & Keupp, H. (2014). Taphonomic traits of clay hosted early Cambrian Burgess Shale-type fossil Lagerstätten in South China. *Palaeogeography, Palaeoclimatology, Palaeoecology*, 398, 59–85.
- Freire, P. T. C., Abagaro, B. T., Souza-Filho, F. E., da Silva, J. H., Saraiva, A. A. F., Brito, D. D., et al. (2013). Pyritization of fossils from Lagerstätte Araripe Basin, Northeast Brazil, from the Cretaceous Period. In N. Whitley & P. T. Vinsen (Eds.), *Pyrite: Synthesis, characterization and uses* (pp. 123–140). New York: Nova Science.
- Freire, P. T. C., Silva, J. H., Sousa-Filho, F. E., Abagaro, B. T., Viana, B. C., Saraiva, G. D., et al. (2014). Vibrational spectroscopy and X-ray diffraction applied to the study of Cretaceous fish fossils from Araripe Basin, Northeast of Brazil. *Journal of Raman Spectroscopy*, 45, 1225–1229.
- Goldhaber, M. B. (1983). Experimental study of metastable sulfur oxyanion formation during pyrite oxidation at pH 6–9 and 30 °C. *American Journal Science*, 283, 193–217.
- Greenwalt, D. E., Rose, T. R., Siljeström, S. M., Goreva, Y. S., Constenius, K. N., & Wingerath, J. G. (2015). Taphonomy of the fossil insects of the middle Eocene Kishenehn Formation. *Acta Palaeontologica Polonica*, 60(4), 931–947.
- Grimaldi, D. A. (1990). *Insects from the Santana Formation, Lower Cretaceous, of Brazil*. New York: Bulletin of AMNH.
- Heads, S. W., & Martins-Neto, R. G. (2007). Orthoptera: Grasshoppers, crickets, locusts and stick insects. In D. M. Martill, G. Bechly, & R. F. Loveridge (Eds.), *The Crato Fossil beds of Brazil: Window into an Ancient World* (pp. 262–265). Cambridge: Cambridge University Press.
- Heimhofer, U., Ariztegui, D., Lenniger, M., Hesselbo, S. P., Martill, D. M., & Rios-Netto, A. M. (2010). Deciphering the depositional environment of the laminated Crato fossil beds (early Cretaceous, Araripe Basin, north-eastern Brazil). *Sedimentology*, 57, 677–694.
- Heimhofer, U., & Martill, D. M. (2007). The sedimentology and depositional environment of the Crato Formation. In D. M. Martill, G. Bechly, & R. F. Loveridge (Eds.), *The Crato Fossil Beds of Brazil: Window into an Ancient World* (pp. 44–63). Cambridge: Cambridge University Press.
- Herdman, J. D., Connelly, B. C., Smooke, M. D., Long, M. B., & Miller, J. H. (2011). A comparison of Raman signatures and laser-induced incandescence with direct numerical simulation of soot growth in non-premixed ethylene/air flames. *Carbon*, 49, 5298–5311.
- Jehlička, J., Urban, O., & Pokorný, J. (2003). Raman spectroscopy of carbon and solid bitumens in sedimentary and metamorphic rocks. *Spectrochimica Acta A*, 59, 2341–2352.
- Laflamme, M., Schiffbauer, J. D., Narbonne, G. M., & Briggs, D. E. G. (2011). Microbial biofilms and the preservation of the Ediacara biota. *Lethaia*, 44, 203–213.
- Li, S., & Hihara, L. H. (2015). A micro-Raman spectroscopic study of marine atmospheric corrosion of carbon steel: The effect of akaganeite. *Journal of the Electrochemical Society*, 162(9), 495–502.
- Littke, R., Klussmann, U., Krooss, B., & Leythaeuser, D. (1991). Quantification of loss of calcite, pyrite, and organic matter due to weathering of Toarcian black Shales and effects on kerogen and bitumen characteristics. *Geochimica et Cosmochimica Acta*, 55, 3369–3378.
- Martill, D. M., & Bechly, G. (2007). Introduction to the Crato Formation. In D. M. Martill, G. Bechly, & R. F. Loveridge (Eds.), *The Crato Fossil beds of Brazil: Window into an Ancient World* (pp. 3–7). Cambridge: Cambridge University Press.
- Martill, D. M., & Heimhofer, U. (2007). Stratigraphy of the Crato Formation. In D. M. Martill, G. Bechly, & R. F. Loveridge (Eds.), *The Crato Fossil beds of Brazil: Window into an Ancient World* (pp. 25–43). Cambridge: Cambridge University Press.
- Martill, D. M., Loveridge, R., & Heimhofer, U. (2007). Halite pseudomorphs in the Crato Formation (Early Cretaceous, Late Aptian—Early Albian), Araripe Basin, northeast Brazil: further evidence for hypersalinity. *Cretaceous Research*, 28, 613–620.
- Martínez-Delclòs, X., Briggs, D. E. G., & Peñalver, E. (2004). Taphonomy of insects in carbonates and amber. *Palaeogeography, Palaeoclimatology, Palaeoecology*, 203, 19–64.
- Martínez-Delclòs, X., & Martinell, J. (1993). Insect taphonomy experiments: Their application to the Cretaceous outcrops of lithographic limestones from Spain. *Kaupia: Darmstader Beiträge zur Naturgeschichte*, 2, 133–144.
- Matos, R. M. D. (1999). History of the northeast Brazilian rift system: Kinematic implications for the break-up between Brazil and West Africa. In N. R. Cameron, R. H. Bate, & V. S. Clure (Eds.), *The oil*

- and gas habitats of the South Atlantic (pp. 55–73). London: Geological Society.
- McNamara, M. E. (2013). The taphonomy of colour in fossil insects and feathers. *Palaeontology*, *56*(3), 557–575.
- McNamara, M. E., Briggs, D. E. G., Orr, P. J., Noh, H., & Cao, H. (2012). The original colours of fossil Beetles. *Proceedings of the Royal Society B*, *279*, 1114–1121.
- McNamara, M. E., Briggs, D. E. G., Orr, P. J., Wedmann, S., Noh, H., & Cao, H. (2011). Fossilized biophotonic nanostructures reveal the original colors of 47-million-year-old moths. *PLoS Biology*, *9*(11), 1001200.
- Menon, F., & Martill, D. M. (2007). Taphonomy and preservation of Crato Formation arthropods. In D. M. Martill, G. Bechly, & R. F. Loveridge (Eds.), *The Crato Fossil beds of Brazil: Window into an Ancient World* (pp. 79–94). Cambridge: Cambridge University Press.
- Morais Neto, J. M., Hegarty, K., & Kerner, G. D. (2005–2006). Abordagem preliminar sobre paleotemperatura e evolução do relevo da Bacia do Araripe, Nordeste do Brasil, a partir da análise de traços de fissão em apatita. *Boletim de Geociências da Petrobras*, *14*, 113–119.
- Moses, C. O., & Herman, J. S. (1991). Pyrite oxidation at circumneutral pH. *Geochimica et Cosmochimica Acta*, *55*, 471–482.
- Moses, C. O., Nordstrom, D. K., Herman, J. S., & Mills, A. L. (1987). Aqueous pyrite oxidation by dissolved oxygen and by ferric iron. *Geochimica et Cosmochimica Acta*, *51*, 1561–1571.
- Nascimento, D. R., Jr., Silva Filho, W. F., Freire, J. G., Jr., & Santos, F. H. (2016). Syngenetic and diagenetic features of evaporite-lutite successions of the Ipubi Formation, Araripe Basin, Santana do Cariri, NE Brazil. *Journal of South American Earth Sciences*, *72*, 315–327.
- Neumann, V. H., Borrego, A. G., Cabrera, L., & Dinod, R. (2003). Organic matter composition and distribution through the Aptian–Albian lacustrine sequences of the Araripe Basin, northeastern Brazil. *International Journal of Coal Geology*, *54*, 21–40.
- Osés, G. L., Petri, S., Becker-Kerber, B., Romero, G. R., Rizzutto, M. A., Rodrigues, F., et al. (2016). Deciphering the preservation of fossil insects: a case study from the Crato Member, Early Cretaceous of Brazil. *PeerJ*, *4*, 1–28.
- Osés, G. L., Petri, S., Voltani, C. G., Prado, G. M., Douglas, G., Rizzutto, M. A., et al. (2017). Deciphering pyritization-kerogenization gradient for fish soft-tissue preservation. *Scientific Reports*, *7*, 1–15.
- Pan, Y., Sha, J., & Fürsich, F. T. (2014). A model for organic fossilization of the early Cretaceous Jehol *lagerstätte* based on the taphonomy of *Ephemeroptera*. *Palaios*, *29*, 363–377.
- Perardi, A., Zoppi, A., & Castellucci, E. (2000). Micro-Raman spectroscopy for standard and in situ characterisation of painting materials. *Journal of Cultural Heritage*, *1*, 269–272.
- Ponte, F., & Ponte Filho, F. (1996). *Evolução tectônica e classificação da Bacia do Araripe*. *Boletim do 4º Simpósio sobre o Cretáceo do Brasil UNESP* (pp. 123–133). São Paulo: Campus de Rio Claro.
- Raff, E. C., Schollaert, K. L., Nelson, D. E., Donoghue, P. C. J., Thomas, C. W., Turner, F. R., et al. (2008). Embryo fossilization is abiological process mediated by microbial biofilms. *Proceedings of the National Academy of Sciences of the United States of America*, *105*, 19360–19365.
- Raiswell, R., Whaler, K., Dean, S., Coleman, M. L., & Briggs, D. E. G. (1993). A simple three-dimensional model of diffusion-with-precipitation applied to localized pyrite formation in framboids, fossils and detrital iron minerals. *Marine Geology*, *113*, 89–100.
- Sadezky, A., Muckenhuber, H., Grothe, H., Niessner, R., & Poeschl, U. (2005). Raman microspectroscopy of soot and related carbonaceous materials: Spectral analysis and structural information. *Carbon*, *43*, 1731–1742.
- Sagemann, J., Bale, S. J., Briggs, D. E. G., & Parkes, R. J. (1990). Controls on the formation of authigenic minerals in association with decaying organic matter: an experimental approach. *Geochimica et Cosmochimica Acta*, *63*, 1083–1095.
- Santos, F. H., Azevedo, J. M., Nascimento, D. R., Jr., Souza, A. C. B., Mendes, M., Bezerra, F. I., et al. (2017). Análise de fácies e petrografia de uma seção do Membro Crato em Nova Olinda (CE): Contribuições à história deposicional e diagenética do neopliano na Bacia do Araripe. *Geologia USP Série Científica*, *17*, 3–18.
- Schiffbauer, J. D., & Laflamme, M. (2012). *Lagerstätten* through time: a collection of exceptional preservational pathways from the terminal Proterozoic through today. *Palaios*, *27*, 275–278.
- Schiffbauer, J. D., Xiao, S., Cai, Y., Wallace, A. F., Hua, H., Hunter, J., et al. (2014). A unifying model for Neoproterozoic–Palaeozoic exceptional fossil preservation through pyritization and carbonaceous compression. *Nature Communications*, *5*, 1–12.
- Shim, S., & Duffy, T. S. (2002). Raman spectroscopy of Fe₂O₃ to 62 GPa. *American Mineralogist*, *87*, 318–326.
- Singer, P. C., & Stumm, W. (1970). Acidic mine drainage: The rate-determining step. *Science*, *167*, 1121–1123.
- Smith, D. M., Cook, A., & Nufio, C. R. (2006). How physical characteristics of beetles affect their fossil preservation. *Palaios*, *21*, 305–310.
- Smith, D. M., & Moe-Hoffman, A. P. (2007). Taphonomy of Diptera in lacustrine environments: A case study from Florissant Fossil Beds, Colorado. *Palaios*, *22*, 623–629.
- Soares, L. P., Kerber, B. B., Osés, G. L., De Oliveira, A. M., & Pacheco, M. L. (2013). Paleobiologia e evolução: o potencial do registro fósilífero brasileiro. *Revista Espinhaço*, *2*, 24–40.
- Stankiewicz, B. A., Briggs, D. E. G., & Evershed, R. P. (1997). Chemical composition of paleozoic and mesozoic fossil invertebrate cuticles as revealed by pyrolysis-gas chromatography/mass spectrometry. *Energy & Fuels*, *11*, 515–521.
- Stankiewicz, B. A., Scott, A. C., Collinson, M. E., Finch, P., Möhle, B., Briggs, D. E. G., et al. (1998). Molecular taphonomy of arthropod and plant cuticles from the Carboniferous of North America: Implications for the origin of kerogen. *Journal of the Geological Society*, *155*, 453–462.
- Thoene-Henning, J., Smith, D. M., Nufio, C. R., & Meyer, H. W. (2012). Depositional setting and fossil insect preservation: A study of the late Eocene Florissant Formation, Colorado. *Palaios*, *27*, 481–488.
- Truică, G. I., Ditaranto, N., Caggiani, M. C., Mangone, A., Lițescu, S. C., Teodor, E. D., et al. (2014). A multi-analytical approach to amber characterization. *Chemical Papers*, *68*(1), 15–21.
- Vandenbroucke, M., & Largeau, C. (2007). Kerogen origin, evolution and structure. *Organic Geochemistry*, *38*, 719–833.
- Viana, M. S., & Neumann, V. H. (2000). Membro Crato da Formação Santana, Chapada do Araripe, CE. Riquíssimo registro de fauna e flora do Cretáceo. In C. Schobbenhaus, D. A. Campos, E. T. Queiroz, M. Winge, & M. L. C. Berbert-Born (Eds.), *Sítios geológicos e paleontológicos do Brasil* (pp. 262–265). Cambridge: Departamento Nacional da Produção Mineral/Companhia de Pesquisa e Recursos Minerais/Comissão Brasileira de Sítios Geológicos e Paleobiológicos.
- Vogt, H., Chattopadhyay, T., & Stolz, H. J. (1983). Complete first-order Raman spectra of the pyrite structure compounds FeS₂, MnS₂, and SiP₂. *Journal of Physics and Chemistry of Solids*, *44*, 869–873.
- Wang, B., Zhao, F., Zhang, H., Fang, Y., & Zheng, D. (2012). Widespread pyritization of insects in the early Cretaceous Jehol biota. *Palaios*, *27*, 707–711.
- Warren, L. V., Varejão, F. G., Quaglio, F., Simões, M. G., Fürsich, F. T., Poiré, D. G., et al. (2017). Stromatolites from the AptianCrato Formation, a hypersaline lake system in the Araripe Basin, northeastern Brazil. *Fácies*, *63*(3), 1–19.
- Zhehikhin, V. V. (2002). Pattern of insect burial and conservation. In A. P. Rasnitsyn & D. L. Quicke (Eds.), *History of insects* (pp. 17–63). Dordrecht: Kluwer Academic Publisher.